HHS Public Access

Author manuscript

Lab Invest. Author manuscript; available in PMC 2016 September 28.

Published in final edited form as:

Lab Invest. 2015 August ; 95(8): 903–913. doi:10.1038/labinvest.2015.70.

TGFβ1 exacerbates blood-brain barrier permeability in a mouse model of hepatic encephalopathy via upregulation of MMP9 and downregulation of claudin-5

Matthew McMillin[1], **Gabriel Frampton**[1], **Andrew Seiwell**[1], **Nisha Patel**[1], **Amber Jacobs**[2], and **Sharon DeMorrow**[1,3,4]

[1]Department of Internal Medicine, Texas A&M Health Science Center College of Medicine, Temple, Texas, 76504

[2]University of Texas Health Science Center, Houston, Texas, 77030

[3]Baylor Scott & White Health Digestive Disease Research Center, Temple, Texas, 76504

[4]Central Texas Veterans Health Care System, Temple, Texas, 76504

Abstract

Recent studies have found that vasogenic brain edema is present during hepatic encephalopathy following acute liver failure and is dependent upon increased matrix metalloproteinase 9 (MMP9) activity and downregulation of tight junction proteins. Furthermore, circulating transforming growth factor β1 (TGFβ1) is increased following liver damage and may promote endothelial cell permeability. This study aimed to assess if increased circulating TGFβ1 drives changes in tight junction protein expression and MMP9 activity following acute liver failure. Blood-brain barrier permeability was assessed in azoxymethane (AOM)-treated mice at 6, 12, and 18 hours post-injection via Evan's blue extravasation. Monolayers of immortalized mouse brain endothelial cells (bEnd.3) were treated with recombinant TGFβ1 (rTGFβ1) and permeability to fluorescein isothiocyanate-dextran (FITC-dextran), MMP9 and claudin-5 expression were assessed. Antagonism of TGFβ1 signaling was performed *in vivo* to determine its role in blood-brain barrier permeability. Blood-brain barrier permeability was increased in mice at 18 hours following AOM injection. Treatment of bEnd.3 cells with rTGFβ1 led to a dose-dependent increase of MMP9 expression as well as a suppression of claudin-5 expression. These effects of rTGFβ1 on MMP9 and claudin-5 expression could be reversed following treatment with a SMAD3 inhibitor. AOM-treated mice injected with neutralizing antibodies against TGFβ demonstrated significantly reduced blood-brain barrier permeability. Blood-brain barrier permeability is induced in AOM mice via a mechanism involving the TGFβ1-driven SMAD3-dependent upregulation of MMP9 expression and decrease of claudin-5 expression. Therefore, treatment modalities aimed at reducing TGFβ1 levels or SMAD3 activity may be beneficial in promoting blood-brain barrier integrity following liver failure.

CORRESPONDING AUTHOR INFORMATION: Matthew McMillin, Department of Internal Medicine, Texas A&M Health Science Center, Central Texas Veterans Health Care System, Building 205, 1901 S 1st St Temple, TX 76504, USA; mcmillin@medicine.tamhsc.edu; Phone: 254-899-7524; Fax: 254-743-0378.

DISCLOSURE/DUALITY OF INTEREST: The authors have no conflicts of interest to disclose.

Acute liver failure (ALF) can lead to many detrimental effects outside the liver, including a systemic inflammatory response, increased energy expenditure and catabolism, and multi-organ failure(1-3). However, one of the most difficult to treat complications of ALF arises from the development of neurological deficits, called hepatic encephalopathy (HE). HE has classically been identified as a reduction of the liver's ability to metabolize neurotoxins, such as ammonia, which accumulate in the brain generating neurological impairment(4). Associated with cerebral ammonia accumulation is cytotoxic brain edema and the development of Alzheimer's Type II astrocytes in the basal ganglia of HE patients(5). However, for neurotoxic metabolites to enter the brain, the blood-brain barrier (BBB), which is not permeable to these neurotoxins in normal physiological conditions, must be disrupted(6).

Microvascular endothelial cells that line the vasculature of the BBB are different from other endothelial cells as they lack fenestrations, have more extensive tight junctions, and have reduced pinocytic vesicular transport(7). Tight junctions, which are functional barriers created by joining together endothelial cells, are made up of cytoplasmic accessory proteins (zona occludens-1, -2, and -3), which anchor the actin cytoskeleton to transmembrane proteins (claudins and occludin)(8). While direct dysregulation of tight junctions can cause vasogenic edema, matrix metalloproteinases (MMPs) have been demonstrated to digest tight junction proteins, allowing for multiple levels of BBB dysregulation(9). During ALF, decreased zona occludens-2 protein expression has been shown to precede BBB permeability(10). Furthermore, it has been shown that claudin-5 and occludin are decreased in mice with HE(11). MMP9 upregulation has also been identified to induce BBB permeability during the later stages of HE(12). However, the specific signaling pathways influencing BBB permeability during HE are not well classified and warrant investigation.

Transforming growth factor beta 1 (TGFβ1) is a signaling protein involved in many processes including immune system modulation, cell proliferation, cell differentiation, and apoptosis(13, 14). During HE it has been shown that TGFβ1 is found in the circulation of rats with hepatic failure(15). Furthermore, we have found TGFβ1 present in the serum of mice following toxic liver injury(16). In regards to BBB permeability, evidence exists that TGFβ1 can directly affect endothelial cell permeability. Endothelial lung cells grown on monolayers treated with TGFβ1 demonstrated significantly increased permeability following treatment(17). Also, retinal endothelial cells treated with TGFβ1 were found to increase MMP9 expression, which increased permeability of these endothelial cells(18).

The hypothesis of this study is that the BBB is disrupted during HE and that circulating TGFβ1 contributes to increased vascular permeability via the upregulation of MMP9 and disruption of tight junction proteins. These combined mechanisms would allow a greater degree of toxin entry into the brain and exacerbate the pathogenesis of HE.

MATERIALS AND METHODS

Materials

Immortalized mouse brain endothelial cells (bEnd.3 cells) were purchased from American Type Culture Collection (Manassas, VA). The 24-well transwell inserts were purchased from

Corning (Tewksbury, MA). Antibodies against MMP9 were purchased from Santa Cruz Biotechnology (Santa Cruz, CA). Antibodies against claudin-5 were purchased from Invitrogen (Grand Island, NY). Antibodies against albumin used for immunocytochemistry were purchased from Genetex (Irvine, CA). Antibodies against albumin for tissue immunohistochemistry were bought from Bethyl Laboratories (Montgomery, TX). Neutralizing antibodies for TGFβ (antiTGFβ) and recombinant TGFβ1 protein (rTGFβ1) were purchased from R&D systems (Minneapolis, MN). SMI71 antibodies, were purchased from Covance (Princeton, NJ). All quantitative PCR primers were purchased from SABiosciences (Frederick, MD). The TGFβ receptor II (TGFβRII) antagonist, GW788388, was purchased from Tocris Bioscience (Minneapolis, MN). All other chemicals were purchased from Sigma-Aldrich (St. Louis, MO) unless otherwise noted, and were of the highest grade available.

Experimental Animals and Hepatic Encephalopathy Model

Mouse *in vivo* experiments were performed using male C57Bl/6 mice (25-30g; Charles River Laboratories, Wilmington, MA). Mice were allowed free access to drinking water and standard mouse chow and were housed in constant temperature, humidity, and 12 hour light-dark cycling. Cages were assigned to random groups and mice received either a single intraperitoneal injection of 100mg/kg AOM to induce ALF and HE or an equal amount of saline for control animals. After injection, mice were placed on heating pads set to 37°C and under heating lamps to ensure they maintained normal body temperature. Further, mice were supplied with hydrogel and rodent chow on their cage floor to ensure they had access to food and hydration. After the first 12 hours, and every subsequent 4 hours, mice were injected subcutaneously with 500μl of a 5% dextrose solution to prevent hypoglycemia. Mice were removed from the study if they underwent a 20% weight loss. Neurological and behavioral assessments of the mice were performed as previously described(16, 19).

In order to suppress the activity of circulating TGFβ, TGFβ-neutralizing antibodies (R&D Systems, Minneapolis, MN) were administered via a single intraperitoneal injection at 1mg/kg 2 hours prior to AOM injection. This treatment has previously been shown to delay the onset of neurological symptoms after AOM injection(16). For this study, no differences were detected between mice treated with AOM alone and mice treated with AOM and immunoglobulin G1 (unpublished observations); therefore mice treated with AOM alone were appropriate controls for mice co-treated with AOM and TGFβ-neutralizing antibodies. Mice in all groups were euthanized at 18 hours following AOM injection. All experiments performed complied with the Scott & White Memorial Hospital IACUC regulations on animal experiments (protocol #2012-019-R).

In vivo BBB permeability measurements

To assess *in vivo* permeabilization of the BBB in the AOM mouse model of HE, a modified Evan's blue dye assay was performed in vehicle and AOM mice(20, 21). Mice were anesthetized with isoflurane inhalation and an incision was made in the neck to expose the carotid artery. Evan's blue dye was injected (5mg/ml; 500μl) and allowed to circulate for 20 minutes at which time mice were euthanized. Euthanized mice were then perfused transcardially with 50ml of cold phosphate buffered saline (PBS), the meninges were

removed, and the brain was blotted dry. The brain stem and cerebellum were removed and the two remaining hemispheres were homogenized with 1.5ml ice-cold trichloroacetic acid (50% v/v) in a glass homogenizer. The resulting homogenates were centrifuged for 10 minutes at 10,000g and absorbance of the supernatant was read at 620nm. *In vivo* permeabilization was measured using the same methods in mice treated with neutralizing antibodies against TGFβ as well.

In vitro permeability assessments

In order to assess endothelial cell permeabilization *in vitro*, monolayers of bEnd.3 cells were seeded at a density of 5.0×10^4 cells/cm^2 onto 24-well Transwell™ inserts with a 0.4μm pore. After cells grew into a confluent monolayer (48-72 hours), cells were treated with AOM (100ng/ml to 10μg/ml), rTGFβ1 (0.5ng/ml to 5.0ng/ml), GW788388 (1μM), specific inhibitor of SMAD3 (SIS3) (1μM), or dimethyl sulfoxide (DMSO) for 24 hours. Following treatment, inserts and chambers were washed with PBS and media was replaced with phenol-red free media. 10kDa FITC-dextran (10mg/ml; 10μl) was added to the upper wells for one hour. Fluorescence (excitation 494nm; emission 520nm) was read in the upper and lower chambers and the permeability coefficient was determined using the following formula(22): $P_{dextran} = (RFU^{lower}/RFU^{upper})(V)(1/t)(1/A)$, where RFU is the relative fluorescent units in the upper and lower wells, V is the volume of the bottom well, t is the time that the FITC-dextran was allowed to diffuse and A is the total surface area of the monolayer (cm^2). Permeability coefficients were normalized by setting basal cell monolayers to a value of 1 to minimize variability between trials.

Immunofluorescence and Immunohistochemistry

For brain immunohistochemistry, free-floating 30μm sections were sectioned and put into 12-well plates containing PBS. Sections were put in 0.5% hydrogen peroxide to quench endogenous peroxidase activity. Brain sections were blocked in 5% goat serum prior to overnight incubation of specific antibodies against albumin(21). Secondary antibodies and DAB peroxidase substrate were supplied from Vector Labs (Burlingame, CA). Incubations and staining development were performed according to the manufacturers' protocols. The sections were viewed using an Olympus BX40 microscope with an Olympus DP25 imaging system (Olympus, Center Valley, PA).

Free-floating immunofluorescence of the brain was performed on 30μm sections. Brains were initially blocked in 5% goat serum prior to overnight incubation with specific antibodies against albumin and SMI71. Immunocytochemistry in bEnd.3 cells was performed using the same methods with antibodies against MMP9 and claudin-5. Immunoreactivity was visualized using Dylight 488- or Cy3-conjugated secondary antibodies and counterstained with 4',6-diamidino-2-phenylindole (DAPI). Slides were viewed and imaged using a Leica TCS SP5-X inverted confocal microscope (Leica Microsystems, Buffalo Grove, IL).

Quantitative PCR

RNA was extracted from bEnd.3 cells using the RNeasy mini kit from Qiagen (Valencia, CA) as per manufacturer's protocols. RNA content of isolated samples was calculated using

a Thermo Scientific Nanodrop 2000 (Rockford, IL). An iScript™ cDNA synthesis kit (Bio-Rad, Hercules, CA) was used to amplify 1μg of RNA per reaction in a MyCycler™ thermal cycler (Bio-Rad). cDNA was loaded onto 96 well plates with iTaq universal SYBR green supermix (Bio-Rad) along with commercially available primers designed against mouse claudin-5, MMP9, and glyceraldehyde 3-phosphate dehydrogenase (GAPDH). Quantitative PCR (qPCR) was performed using a Strategene Mx3005P qPCR system (Santa Clara, CA) and a ΔΔCT analysis was performed using basal bEnd.3 cells as controls(23, 24). Data for all experiments are expressed as mean relative mRNA levels ± SEM (n=4).

Immunoblotting

Homogenization of bEnd.3 cells was accomplished by scraping cells in lysis buffer supplemented with 1% protease inhibitor cocktail. Protein content in cell lysates from bEnd. 3 cells was quantitated using a BCA protein assay (Thermo Scientific, Rockford, IL). SDS-PAGE gels were loaded with 10-20μg of protein diluted in Laemmli buffer per each tissue sample. Specific antibodies against claudin-5, MMP9, and β-actin were used. All imaging was performed on an Odyssey 9120 Infrared Imaging System (LI-COR, Lincoln, NE). Data are expressed as fold change in fluorescent band intensity of target antibody divided by the loading control, β-actin. The values of basal bEnd.3 cells were used as a baseline and set to a relative protein expression value of 1. All treatment groups were expressed as changes of fluorescent band intensity of target antibody to β-actin relative to basal. All band intensity quantifications were performed using ImageJ software (National Institutes of Health, Bethesda, MD). Data for all experiments are expressed as mean relative protein ± SEM (n=4).

Statistical Analysis

All statistical analyses were performed using Graphpad Prism software (Graphpad Software, La Jolla, CA). Results were expressed as mean ± SEM. For data that passed normality tests, the Student's t-test was used when differences between two groups were analyzed, and analysis of variance used when differences between three or more groups were compared followed by the appropriate post hoc test. If tests for normality failed, two groups were compared with a Mann-Whitney U test. When tests for normality failed with more than 2 groups, a Kruskal-Wallis ranked analysis was used. Differences were considered significant when the p value was less than 0.05.

RESULTS

The BBB is disrupted following AOM-induced liver failure

C57Bl/6 mice were treated with the hepatotoxin AOM and Evan's blue extravasation was assessed after 6, 12 or 18 hours. Mice that were treated for 18 hours with AOM had significantly increased Evan's blue dye present in their brains compared to those perfused with dye alone (figure 1A). Interestingly, mice that underwent Evan's blue extravasation assays at 6 and 12 hours post AOM injection had essentially no change in Evan's blue dye penetrance into their brain compared to untreated mice. As Evan's blue binds albumin, this provides evidence that the BBB is being disrupted to a large enough degree to allow the passage of large proteins into the brain following ALF. Representative pictures of untreated,

0-12 hours, and 18-hour brains support the findings from our absorbance measures (figure 1B). Albumin immunofluorescence was performed in the cortex of vehicle and AOM mice. This demonstrated that in vehicle mice there is only slight residual albumin staining in cerebral microvessels while in AOM-treated mice albumin immunoreactivity is found diffusely throughout the tissue (figure 1C). Together, these findings demonstrate that BBB permeability is increased in mice treated with AOM as is indicated by the presence of both Evan's blue dye and positive albumin immunofluorescence in the cortex during later stages of AOM-induced HE.

Circulating TGFβ1 can disrupt the BBB

Initially the effects of AOM treatment on endothelial cell permeability were assessed using confluent bEnd.3 monolayers in transwell chambers as an *in vitro* model of the BBB. Treatment of bEnd.3 monolayers with 100ng/ml to 10μg/ml of AOM did not increase monolayer permeability as assessed by diffusion of 10 kDa FITC-dextran across the transwell (figure 2A). Therefore, it appears that some other circulating factor that is released during AOM-induced hepatotoxicity contributes to increased BBB permeability observed following AOM treatment. In order to determine if TGFβ1 could induce permeability, monolayers were treated with increasing doses of rTGFβ1 and permeability was assessed. At doses of 1.0ng/ml and 5.0ng/ml of rTGFβ1, which are physiologically relevant levels in mice(25), there were significant increases in BBB permeability (figure 2B). To ensure that the resulting increased permeabilization was entirely due to TGFβ1 signal transduction, monolayers were treated with rTGFβ1 in combination with a TGFβRII antagonist, GW788388. The previously seen increased permeability of 1.0ng/ml rTGFβ1-treated bEnd.3 monolayers was significantly reduced following treatment with 1μM GW788388 (figure 2C). This demonstrates that TGFβ1 receptor-mediated signaling is responsible for the effects of TGFβ1 on inducing brain endothelial cell monolayer permeability.

MMP9 is upregulated in endothelial cells by TGFβ1

In order to determine if TGFβ1-induced increase in brain endothelial cell permeability was due to an increase of MMP9 activity, bEnd.3 cells were treated with rTGFβ1 and MMP9 expression assayed. Treatment with rTGFβ1 led to a dose-dependent increase of MMP9 mRNA expression, with treatments of 0.5ng/ml rTGFβ1 and higher generating a significant increase (figure 3A). To determine if this treatment led to increased protein levels of MMP9, immunofluorescence was performed and a dose-dependent increase in MMP9 immunostaining was observed (figure 3B). Quantification of MMP9 immunofluorescence determined that doses of 1.0ng/ml and 5.0ng/ml of rTGFβ1 led to a significant increase in immunoreactivity (figure 3C). These data demonstrate that TGFβ1 may generate its effects on permeability through upregulation of MMP9.

Claudin-5 is downregulated by TGFβ1 in bEnd.3 cells

Since TGFβ1 was shown to increase permeability of bEnd.3 monolayers and induce an upregulation of MMP9, further investigation into tight junction protein regulation was warranted. The tight junction proteins claudin-5, occludin, zona occludens-1, and zona occludens-2 were assessed following rTGFβ1 treatment. There were no significant changes in occludin, zona occludens-1, and zona occludens-2 expression when assessed by western

blotting, qPCR, or immunofluorescence (data not shown). However, there were changes observed in claudin-5. Treatment of bEnd.3 cells with rTGFβ1 led to a significant suppression of claudin-5 mRNA expression (figure 4A). This effect translated into a reduction of claudin-5 protein with significant suppression at doses of 0.5ng/ml rTGFβ1 and greater (figure 4B). In order to determine if these changes in gene and protein expression led to a functional disruption of the tight junction, immunofluorescence against claudin-5 was performed, demonstrating staining localized to the cell membrane of basal cells. However, when bEnd.3 cells were treated with rTGFβ1, claudin-5 immunostaining became increasingly cytoplasmic as doses increased, indicating a disruption of tight junctions (figure 4C). These data demonstrate that TGFβ1 is able to downregulate claudin-5 and disrupt its localization to tight junctions in brain endothelial cells.

Modulations of MMP9 and claudin-5 via TGFβ1 are dependent on SMAD3

SMAD3 is one of the intracellular proteins that transduce extracellular signaling of TGFβ1 to the nucleus, thereby, generating effects on transcription(26). To determine if TGFβ1 is exerting its effects through a SMAD3-dependent mechanism, bEnd.3 cells were treated with rTGFβ1 and the SMAD3 antagonist SIS3. Treatment of monolayers with TGFβ1 and SIS3 was able to alleviate the permeability caused due to TGFβ1 treatment alone (figure 5A). Treatment of bEnd.3 cells with TGFβ1 and SIS3 significantly reduced MMP9 mRNA expression to near the levels of basal cells (figure 5B). Furthermore, pretreatment with SIS3 alleviated the TGFβ1-induced increase in MMP9 immunoreactivity (figure 5C). Quantification of MMP9 immunofluorescence determined that treatment with the SMAD3 inhibitor was able to significantly reduce MMP9 immunoreactivity in bEnd.3 cells to near basal levels (figure 5D).

In addition to the effects of SMAD3 antagonism on MMP9, treatment with both TGFβ1 and SIS3 was also able to rescue the downregulation of claudin-5 mRNA and protein (figures 6A and 6B) compared to TGFβ1 treatment alone. In order to determine if disruption of claudin-5 cellular localization was dependent upon SMAD3, coverslips of bEnd.3 cells were treated with rTGFβ1 and SIS3. Treatment of bEnd.3 cells with SIS3 was able to partially restore the localization of claudin-5 to the cell membrane (figure 6C). Together, these findings demonstrate that the upregulation of MMP9 and downregulation of claudin-5 via TGFβ1 in brain endothelial cells is dependent upon SMAD3.

In vivo neutralization of TGFβ1 reduces BBB permeability following liver failure

An Evan's blue extravasation assay was performed in mice treated with AOM and/or neutralizing antibodies against TGFβ for 18 hours. Mice injected with AOM demonstrated a significant increase in Evan's blue dye in their brain. This increase was significantly reduced if the mice were pretreated with neutralizing antibodies against TGFβ (figure 7A). Representative pictures of the brains of mice treated with AOM and/or neutralizing antibodies against TGFβ support these results (figure 7B). To demonstrate this effect more conclusively, immunohistochemistry was performed against albumin in the brains of mice treated with AOM and neutralizing antibodies against TGFβ. This immunohistochemistry displays a significant elevation of albumin in the cortex of AOM mice, which is reduced in mice treated with neutralizing antibodies against TGFβ (figure 7C). In order to visualize

brain endothelial cells, immunofluorescence staining was performed for the endothelial cell marker SMI71. AOM-treated mice show discontinuous staining for SMI71 while mice pretreated with neutralizing antibodies against TGFβ show continuous staining similar to vehicle-treated mice (figure 7D). These data support our hypothesis that inhibiting circulating TGFβ1 activity *in vivo* is able to restore BBB function following ALF.

DISCUSSION

This manuscript reports that 18 hours following AOM injection the BBB is significantly disrupted, as measured by Evan's blue dye extravasation. Investigation into the molecular mechanisms that drive this effect determined that brain endothelial cells have increased MMP9 expression and reduced claudin-5 expression following treatment with rTGFβ1. The increase in MMP9 expression and suppression of claudin-5 was found to be dependent upon SMAD3 signaling, as treatment with the SMAD3 inhibitor SIS3 was able to reverse the effects of rTGFβ1 treatment. Finally, inhibition of circulating TGFβ1 in AOM-treated mice by injection of neutralizing antibodies was able to reduce albumin infiltration in the brain, reduce microvessel disruption, and significantly reduce BBB permeability compared to mice treated with AOM alone. A working model of our findings is presented in figure 8.

This study demonstrates that the AOM model of HE generates a significant disruption of the BBB as measured by the presence of Evan's blue dye in the cerebral cortices of AOM-treated mice. Interestingly, this only occurs at later stages of HE when severe neurological decline is present (ataxia and minor reflex deficits are typically observed around twelve hours in this model)(16). Other researchers have performed Evan's blue dye extravasation using a lower dose of AOM (50mg/kg) and have shown similar findings(12). Furthermore, rats treated with D-galactosamine to induce ALF show significant increase of Evan's blue extravasation at coma(27). These findings mirror the more recent reports of vasogenic edema that have been reported in clinical studies in both acute and chronic liver failure(28, 29). However, it has recently been proposed that AOM itself may be leading to a direct effect on the endothelial cells of the BBB. The monolayer experiments performed in this study indicate that AOM does not cause increased endothelial cell permeability directly, but that TGFβ1 contributes to increased monolayer permeability in this model. One research group has investigated AOM in an endothelial cell and astrocyte co-culture model and found that treatment with 5μg/ml AOM for 24 hours leads to increased endothelial cell permeability(30). The discrepancy in the effects of AOM on permeability may lie in the site of AOM administration. The previous study administered AOM in the media between the astrocyte and endothelial cell layer rather than directly onto the endothelial cells themselves (as would mimic the *in vivo* situation). The increased permeability, therefore, may be a reflection of direct toxicity of AOM on astrocytes, which may subsequently release factors that increase the endothelial cell permeability. However, these direct effects of AOM would not translate *in vivo* as the toxin would have to already cross the BBB to generate this effect. These conclusions about AOM not generating direct toxicity on BBB endothelial cells *in vivo* are also supported by AOM-treated mice not showing BBB permeability to near coma, as is reported in this study and by others(12).

The current study demonstrated that MMP9 expression was increased in bEnd.3 cells following treatment with rTGFβ1. TGFβ1 treatment has been shown to lead to increased expression of MMP9 in corneal epithelial cells(31) and in podocytes(32). MMP9 plays many roles in dysregulation of the BBB as it has the capability to degrade claudin-5, occludin, zona occludens-1, and zona occludens-2(9). During AOM-induced HE, the upregulation of MMP9 has been shown to disrupt tight junction expression and pharmacological inhibition of MMP9 restores tight junction protein expression to near control levels(11). Interestingly, it has also been shown that treatment of rat brain microvascular endothelial cells with ammonia alone is able to induce MMP9 expression(33). Therefore, it is conceivable that TGFβ1 could potentially be acting in synergy with ammonia to induce MMP9 expression and further drive BBB permeability. Further studies are necessary to identify the specific cellular sources, regulation, and protein interactions of MMP9 to better understand its role in BBB dysfunction following liver failure.

Previous research into the effects of ALF on tight junction protein dysregulation has been conflicting. One group of researchers found that AOM-treated mice have disruptions of occludin, claudin-5, zona occludens-1, and zona occludens-2 protein expression as assessed with western blots(11). Conversely, other researchers have used the AOM model and observed no changes in immunoblot tight junction protein expression(34). Our studies focused only on the effects of TGFβ1 on claudin-5 expression and demonstrated that treatment of bEnd.3 cells with rTGFβ1 downregulated claudin-5 and led to the translocation of this protein from the cell membrane to the cytosol. Claudin-5 downregulation has been shown to lead to increased BBB permeability following hypoxia(35), focal cerebral cooling(36), and ischemia reperfusion injury(37). Also, other studies have found that TGFβ1 can lead to the direct downregulation of claudin-5(38). Thus, these findings support the concept that circulating TGFβ1 promotes the BBB permeability observed *in vivo* primarily through the downregulation of claudin-5. To our knowledge, this is the first study to show changes in both claudin-5 and MMP9 in bEnd.3 cells following treatment with rTGFβ1. However, whether the effects of TGFβ1 on claudin-5 and MMP-9 are part of the same pathway or are the result of two separate TGFβ1-mediated processes is unknown. Regardless, the overall outcome is an increase in BBB permeability as a result of TGFβ1 signaling.

TGFβ1 transduces its signal via activation of its receptor and subsequent phosphorylation of the SMAD proteins, SMAD2 or SMAD3(39). We determined that SMAD3 was generating the majority of the effects that we were seeing both *in vivo* and *in vitro* by showing that treatment with SIS3 was able to reverse the effects of TGFβ1. Interestingly, other studies have inhibited TGFβ receptor kinase activity, which reduced SMAD3 activity, and observed elevated claudin-5 expression(40). In addition, human meningeal cells treated with a SMAD3 inhibitor were able to attenuate TGFβ1-dependent MMP9 upregulation(41). Thus, there is strong evidence supporting dysregulation of both claudin-5 and MMP9 by TGFβ1 via a SMAD3-dependent mechanism. As this was the first study manipulating TGFβ1/SMAD3 signaling in these cells, it is possible that this signaling pathway could be generating other effects on these cells which have not be investigated, such as affecting junctional adhesion molecules or proteins of the adherens junction.

Sequestration of circulating TGFβ1 *in vivo* demonstrated a significant role for TGFβ1 in promoting permeability of the BBB in this model of ALF. One downstream consequence of TGFβ1 is the activation of phosphatidylinositol-3 kinase/Akt pathway signaling(42), which has been demonstrated to promote vascular permeability in cancer models(43, 44). Also, this pathway has been shown to induce BBB permeability following focal cerebral ischemia(45), HIV-induced BBB disruption(46), and traumatic brain injury(47). In addition to this, we have previously identified that inhibition of TGFβ1 can lead to increased expression of the hedgehog transcription factor Gli1(16). Indeed, hedgehog pathway activation has been shown to be protective in experimental autoimmune encephalomyelitis, a mouse model of multiple sclerosis, by promoting blood-brain barrier integrity(48). Also, treatment of mice with polydatin, which elevates Gli1, has been shown to restore BBB function following ischemic insult(49). These findings suggest that inhibiting TGFβ1 could promote BBB integrity via suppression of vascular permeability pathway signaling as well as by inducing factors to promote BBB vascular integrity. Further research into the specific signaling pathways in brain endothelial cells that are dysregulated by TGFβ1 are still warranted and are currently ongoing in the laboratory.

Together, our findings support that TGFβ1 is driving BBB permeability via downregulation of claudin-5 and upregulation of MMP9 and that these effects are dependent upon SMAD3. These results support that manipulations of TGFβ1 or therapies to target SMAD3 may be potential therapeutic targets to treat ALF patients whom have the potential to develop HE.

ACKNOWLEDGEMENTS

The authors would like to acknowledge Dinorah Carrillo for technical assistance on this project.

SOURCES OF SUPPORT: The following study was funded by an NIH R01 award (DK082435), an NIH K01 award (DK078532) and a Scott & White Intramural grant award (No: 050339) to Dr. DeMorrow. This material is the result of work supported with resources and the use of facilities at the Central Texas Veterans Health Care System, Temple, Texas.

ABBREVIATIONS

ALF	acute liver failure
antiTGFβ	neutralizing antibodies for TGFβ
AOM	azoxymethane
BBB	blood brain barrier
bEnd.3	immortalized mouse brain endothelial cells
DAPI	4',6-diamidino-2-phenylindole
DMSO	Dimethyl sulfoxide, vehicle
FITC-dextran	fluorescein isothiocyanate-dextran
GAPDH	glyceraldehyde 3-phosphate dehydrogenase
HE	Hepatic encephalopathy

MMP9	Matrix metalloproteinase 9
PBS	phosphate buffered saline
qPCR	Quantitative PCR
rTGFβ1	recombinant transforming growth factor β1
SIS3	specific inhibitor of SMAD3
SMI71	endothelial cell marker
TGFβ1	Transforming growth factor beta1
TGFβRII	Transforming growth factor β receptor II

REFERENCES

1. Rolando N, Wade J, Davalos M, Wendon J, Philpott-Howard J, Williams R. The systemic inflammatory response syndrome in acute liver failure. Hepatology. 2000; 32(4 Pt 1):734–9. [PubMed: 11003617]
2. Walsh TS, Wigmore SJ, Hopton P, Richardson R, Lee A. Energy expenditure in acetaminophen-induced fulminant hepatic failure. Crit Care Med. 2000; 28(3):649–54. [PubMed: 10752809]
3. Bernal W, Auzinger G, Dhawan A, Wendon J. Acute liver failure. Lancet. 2010; 376(9736):190–201. [PubMed: 20638564]
4. Rama Rao KV, Norenberg MD. Brain energy metabolism and mitochondrial dysfunction in acute and chronic hepatic encephalopathy. Neurochem Int. 2012; 60(7):697–706. [PubMed: 21989389]
5. Hazell AS, Butterworth RF. Hepatic encephalopathy: An update of pathophysiologic mechanisms. Proc Soc Exp Biol Med. 1999; 222(2):99–112. [PubMed: 10564534]
6. Lockwood AH, Yap EW, Wong WH. Cerebral ammonia metabolism in patients with severe liver disease and minimal hepatic encephalopathy. J Cereb Blood Flow Metab. 1991; 11(2):337–41. [PubMed: 1997506]
7. Ballabh P, Braun A, Nedergaard M. The blood-brain barrier: an overview: structure, regulation, and clinical implications. Neurobiol Dis. 2004; 16(1):1–13. [PubMed: 15207256]
8. Hawkins BT, Davis TP. The blood-brain barrier/neurovascular unit in health and disease. Pharmacological reviews. 2005; 57(2):173–85. [PubMed: 15914466]
9. Yang Y, Estrada EY, Thompson JF, Liu W, Rosenberg GA. Matrix metalloproteinase-mediated disruption of tight junction proteins in cerebral vessels is reversed by synthetic matrix metalloproteinase inhibitor in focal ischemia in rat. J Cereb Blood Flow Metab. 2007; 27(4):697–709. [PubMed: 16850029]
10. Shimojima N, Eckman CB, McKinney M, Sevlever D, Yamamoto S, Lin W, et al. Altered expression of zonula occludens-2 precedes increased blood-brain barrier permeability in a murine model of fulminant hepatic failure. J Invest Surg. 2008; 21(3):101–8. [PubMed: 18569429]
11. Chen F, Ohashi N, Li W, Eckman C, Nguyen JH. Disruptions of occludin and claudin-5 in brain endothelial cells in vitro and in brains of mice with acute liver failure. Hepatology. 2009; 50(6): 1914–23. [PubMed: 19821483]
12. Nguyen JH, Yamamoto S, Steers J, Sevlever D, Lin W, Shimojima N, et al. Matrix metalloproteinase-9 contributes to brain extravasation and edema in fulminant hepatic failure mice. J Hepatol. 2006; 44(6):1105–14. [PubMed: 16458990]
13. Yoshimura A, Wakabayashi Y, Mori T. Cellular and molecular basis for the regulation of inflammation by TGF-beta. Journal of biochemistry. 2010; 147(6):781–92. [PubMed: 20410014]
14. Shi Y, Massague J. Mechanisms of TGF-beta signaling from cell membrane to the nucleus. Cell. 2003; 113(6):685–700. [PubMed: 12809600]

15. Eguchi S, Kamlot A, Ljubimova J, Hewitt WR, Lebow LT, Demetriou AA, et al. Fulminant hepatic failure in rats: survival and effect on blood chemistry and liver regeneration. Hepatology. 1996; 24(6):1452–9. [PubMed: 8938180]
16. McMillin M, Galindo C, Pae HY, Frampton G, Di Patre PL, Quinn M, et al. Gli1 activation and protection against hepatic encephalopathy is suppressed by circulating transforming growth factor β1 in mice. J Hepatology. 2014 In Press.
17. Goldberg PL, MacNaughton DE, Clements RT, Minnear FL, Vincent PA. p38 MAPK activation by TGF-beta1 increases MLC phosphorylation and endothelial monolayer permeability. American journal of physiology Lung cellular and molecular physiology. 2002; 282(1):L146–54. [PubMed: 11741826]
18. Behzadian MA, Wang XL, Windsor LJ, Ghaly N, Caldwell RB. TGF-beta increases retinal endothelial cell permeability by increasing MMP-9: possible role of glial cells in endothelial barrier function. Investigative ophthalmology & visual science. 2001; 42(3):853–9. [PubMed: 11222550]
19. McMillin M, Frampton G, Thompson M, Galindo C, Standeford H, Whittington E, et al. Neuronal CCL2 is upregulated during hepatic encephalopathy and contributes to microglia activation and neurological decline. J Neuroinflammation. 2014 In Press.
20. Manaenko A, Chen H, Kammer J, Zhang JH, Tang J. Comparison Evans Blue injection routes: Intravenous versus intraperitoneal, for measurement of blood-brain barrier in a mice hemorrhage model. Journal of neuroscience methods. 2011; 195(2):206–10. [PubMed: 21168441]
21. Quinn M, McMillin M, Galindo C, Frampton G, Pae HY, DeMorrow S. Bile acids permeabilize the blood brain barrier after bile duct ligation in rats via Rac1-dependent mechanisms. Digestive and liver disease : official journal of the Italian Society of Gastroenterology and the Italian Association for the Study of the Liver. 2014; 46(6):527–34.
22. Yuan, SY.; Rigor, RR. Methods for measuring permeability. Regulation of Endothelial Barrier Function. Integrated Systems Physiology: From Molecule to Function to Disease. San Rafael (CA): 2010.
23. DeMorrow S, Francis H, Gaudio E, Venter J, Franchitto A, Kopriva S, et al. The endocannabinoid anandamide inhibits cholangiocarcinoma growth via activation of the noncanonical Wnt signaling pathway. Am J Physiol Gastrointest Liver Physiol. 2008; 295(6):G1150–8. [PubMed: 18832445]
24. Livak KJ, Schmittgen TD. Analysis of relative gene expression data using real-time quantitative PCR and the 2(-Delta Delta C(T)) Method. Methods. 2001; 25(4):402–8. [PubMed: 11846609]
25. Khan SA, Joyce J, Tsuda T. Quantification of active and total transforming growth factor-beta levels in serum and solid organ tissues by bioassay. BMC research notes. 2012; 5:636. [PubMed: 23151377]
26. Heldin CH, Miyazono K, ten Dijke P. TGF-beta signalling from cell membrane to nucleus through SMAD proteins. Nature. 1997; 390(6659):465–71. [PubMed: 9393997]
27. Yamamoto S, Nguyen JH. TIMP-1/MMP-9 imbalance in brain edema in rats with fulminant hepatic failure. The Journal of surgical research. 2006; 134(2):307–14. [PubMed: 16488444]
28. Rai V, Nath K, Saraswat VA, Purwar A, Rathore RK, Gupta RK. Measurement of cytotoxic and interstitial components of cerebral edema in acute hepatic failure by diffusion tensor imaging. Journal of magnetic resonance imaging : JMRI. 2008; 28(2):334–41. [PubMed: 18626948]
29. Kale RA, Gupta RK, Saraswat VA, Hasan KM, Trivedi R, Mishra AM, et al. Demonstration of interstitial cerebral edema with diffusion tensor MR imaging in type C hepatic encephalopathy. Hepatology. 2006; 43(4):698–706. [PubMed: 16557540]
30. Jayakumar AR, Ruiz-Cordero R, Tong XY, Norenberg MD. Brain edema in acute liver failure: role of neurosteroids. Arch Biochem Biophys. 2013; 536(2):171–5. [PubMed: 23567839]
31. Kim HS, Luo L, Pflugfelder SC, Li DQ. Doxycycline inhibits TGF-beta1-induced MMP-9 via Smad and MAPK pathways in human corneal epithelial cells. Investigative ophthalmology & visual science. 2005; 46(3):840–8. [PubMed: 15728539]
32. Huang HC, Liu SY, Liang Y, Liu Y, Li JZ, Wang HY. [Transforming growth factor-beta1 stimulates matrix metalloproteinase-9 production through ERK activation pathway and upregulation of Ets-1 protein]. Zhonghua yi xue za zhi. 2005; 85(5):328–31. [PubMed: 15854510]

33. Skowronska M, Zielinska M, Wojcik-Stanaszek L, Ruszkiewicz J, Milatovic D, Aschner M, et al. Ammonia increases paracellular permeability of rat brain endothelial cells by a mechanism encompassing oxidative/nitrosative stress and activation of matrix metalloproteinases. J Neurochem. 2012; 121(1):125–34. [PubMed: 22260250]
34. Bémeur C, Chastre A, Desjardins P, Butterworth R. No changes in expression of tight junction proteins or blood–brain barrier permeability in azoxymethane-induced experimental acute liver failure. Neurochem Int. 2010; 56(2):205–7.
35. Koto T, Takubo K, Ishida S, Shinoda H, Inoue M, Tsubota K, et al. Hypoxia disrupts the barrier function of neural blood vessels through changes in the expression of claudin-5 in endothelial cells. Am J Pathol. 2007; 170(4):1389–97. [PubMed: 17392177]
36. Inamura A, Adachi Y, Inoue T, He Y, Tokuda N, Nawata T, et al. Cooling treatment transiently increases the permeability of brain capillary endothelial cells through translocation of claudin-5. Neurochem Res. 2013; 38(8):1641–7. [PubMed: 23653089]
37. Jiao H, Wang Z, Liu Y, Wang P, Xue Y. Specific role of tight junction proteins claudin-5, occludin, and ZO-1 of the blood-brain barrier in a focal cerebral ischemic insult. J Mol Neurosci. 2011; 44(2):130–9. [PubMed: 21318404]
38. Ronaldson PT, Demarco KM, Sanchez-Covarrubias L, Solinsky CM, Davis TP. Transforming growth factor-beta signaling alters substrate permeability and tight junction protein expression at the blood-brain barrier during inflammatory pain. J Cereb Blood Flow Metab. 2009; 29(6):1084–98. [PubMed: 19319146]
39. Larsson J, Karlsson S. The role of Smad signaling in hematopoiesis. Oncogene. 2005; 24(37): 5676–92. [PubMed: 16123801]
40. Watabe T, Nishihara A, Mishima K, Yamashita J, Shimizu K, Miyazawa K, et al. TGF-beta receptor kinase inhibitor enhances growth and integrity of embryonic stem cell-derived endothelial cells. J Cell Biol. 2003; 163(6):1303–11. [PubMed: 14676305]
41. Okamoto T, Takahashi S, Nakamura E, Nagaya K, Hayashi T, Fujieda K. Transforming growth factor-beta1 induces matrix metalloproteinase-9 expression in human meningeal cells via ERK and Smad pathways. Biochem Biophys Res Commun. 2009; 383(4):475–9. [PubMed: 19371720]
42. Kato M, Putta S, Wang M, Yuan H, Lanting L, Nair I, et al. TGF-beta activates Akt kinase through a microRNA-dependent amplifying circuit targeting PTEN. Nature cell biology. 2009; 11(7):881–9. [PubMed: 19543271]
43. Hu L, Hofmann J, Jaffe RB. Phosphatidylinositol 3-kinase mediates angiogenesis and vascular permeability associated with ovarian carcinoma. Clin Cancer Res. 2005; 11(22):8208–12. [PubMed: 16299254]
44. Yuan TL, Choi HS, Matsui A, Benes C, Lifshits E, Luo J, et al. Class 1A PI3K regulates vessel integrity during development and tumorigenesis. Proc Natl Acad Sci U S A. 2008; 105(28):9739–44. [PubMed: 18621722]
45. Kilic E, Kilic U, Wang Y, Bassetti CL, Marti HH, Hermann DM. The phosphatidylinositol-3 kinase/Akt pathway mediates VEGF's neuroprotective activity and induces blood brain barrier permeability after focal cerebral ischemia. FASEB journal : official publication of the Federation of American Societies for Experimental Biology. 2006; 20(8):1185–7. [PubMed: 16641198]
46. Yang B, Singh S, Bressani R, Kanmogne GD. Cross-talk between STAT1 and PI3K/AKT signaling in HIV-1-induced blood-brain barrier dysfunction: role of CCR5 and implications for viral neuropathogenesis. J Neurosci Res. 2010; 88(14):3090–101. [PubMed: 20568281]
47. Tchantchou F, Zhang Y. Selective inhibition of alpha/beta-hydrolase domain 6 attenuates neurodegeneration, alleviates blood brain barrier breakdown, and improves functional recovery in a mouse model of traumatic brain injury. J Neurotrauma. 2013; 30(7):565–79. [PubMed: 23151067]
48. Alvarez JI, Dodelet-Devillers A, Kebir H, Ifergan I, Fabre PJ, Terouz S, et al. The Hedgehog pathway promotes blood-brain barrier integrity and CNS immune quiescence. Science. 2011; 334(6063):1727–31. [PubMed: 22144466]
49. Ji H, Zhang X, Du Y, Liu H, Li S, Li L. Polydatin modulates inflammation by decreasing NF-kappaB activation and oxidative stress by increasing Gli1, Ptch1, SOD1 expression and

ameliorates blood-brain barrier permeability for its neuroprotective effect in pMCAO rat brain. Brain Res Bull. 2012; 87(1):50–9. [PubMed: 22001340]

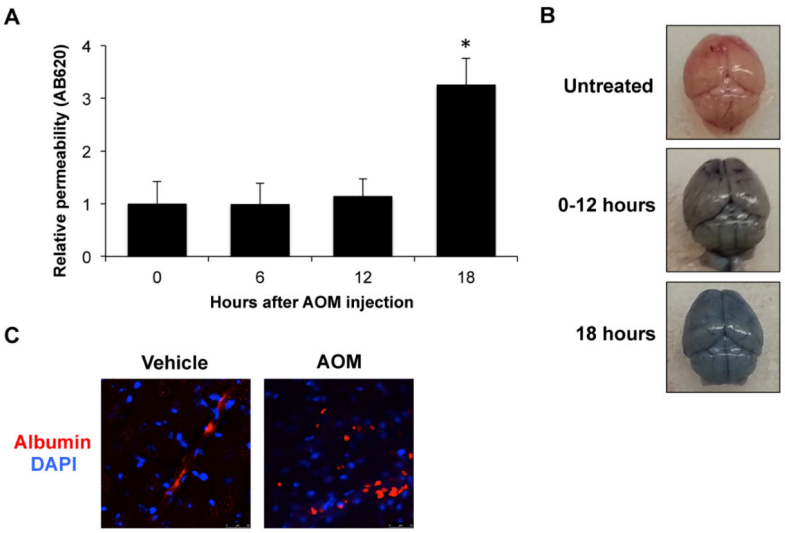

Figure 1. The BBB is disrupted in the later stages of HE

(A) Evan's blue dye permeability assay of AOM mice at indicated timepoints following AOM injection (n=4). Permeability was measured by measuring absorbance of Evan's blue dye (620 nM). (B) Representative pictures of brains from mice that had no Evan's blue dye extravasation (untreated), mice infused with Evan's blue dye after AOM treatment from 0-12 hours, and mice infused with Evan's blue dye 18 hours after AOM injection. (C) Immunofluorescence in vehicle and AOM cortex for albumin (red) and DAPI (blue). Data in the permeability assay are reported as mean ± SEM. *=$p<0.05$ compared to 0 hour mice.

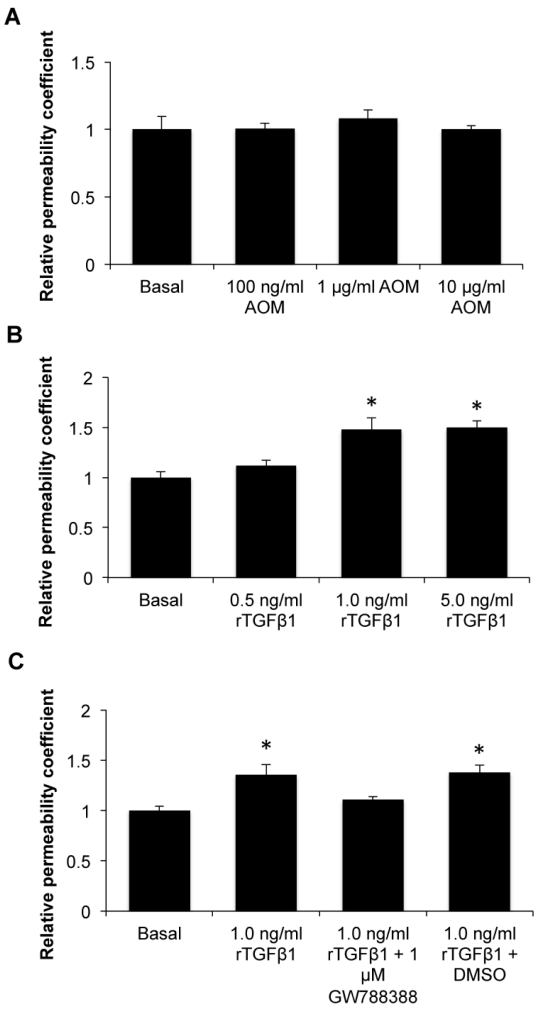

Figure 2. Monolayers of brain endothelial cells are permeabilized by treatment with rTGFβ1

(A) Transwell chambers seeded with a monolayer of bEnd.3 cells were treated with indicated concentrations of AOM for 24 hours. Diffusion of 10-kDa FITC-dextran from the top to bottom chamber and subsequent measurement of fluorescence was employed to assess monolayer permeability. (B) Monolayers of bEnd.3 cells plated on transwells were treated with indicated doses of rTGFβ1 for 24 hours. Permeability was assessed by 10-kDa FITC-dextran diffusion from the top chamber to the bottom chamber and subsequent measurement of fluorescence (Excitation 494/Emission 520). (C) Monolayers of brain endothelial cells were treated with rTGFβ1, the TGFβRII antagonist GW788388, or DMSO (vehicle for GW788388) for 24 hours. Permeability was assessed by measuring diffusion of 10-kDa FITC-dextran from the top chamber to the bottom chamber via fluorescence measurement (Excitation 494/Emission 520). Data in the monolayer assays are reported as mean ± SEM. *=$p<0.05$ compared to basal bEnd.3 cells.

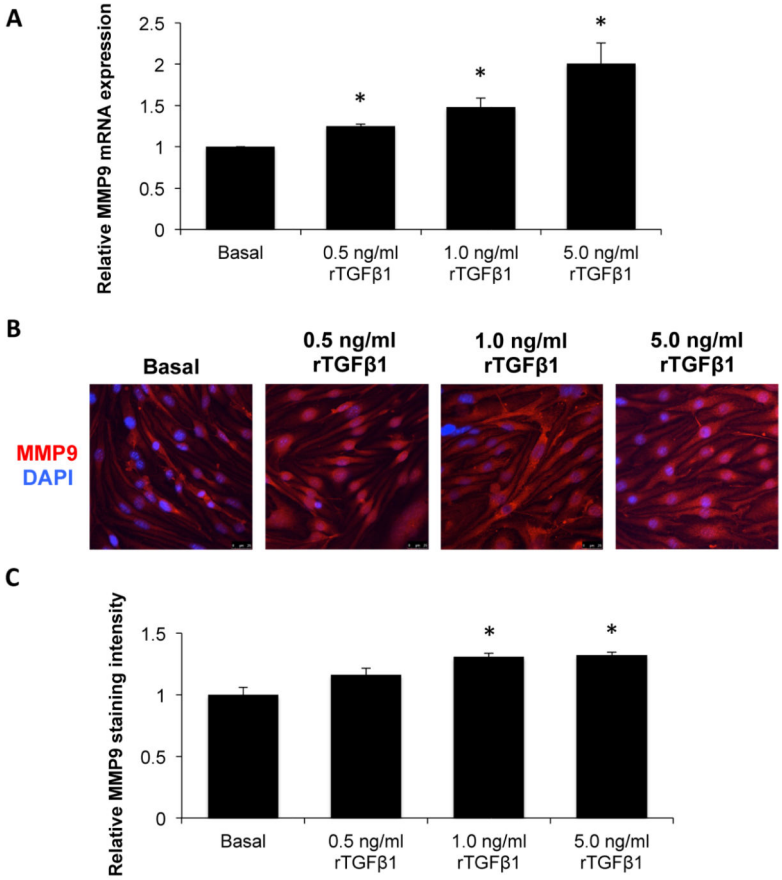

Figure 3. MMP9 is upregulated by TGFβ1 in bEnd.3 cells

(A) MMP9 mRNA expression in bEnd.3 cells as assessed by qPCR following treatment with rTGFβ1. (B) Coverslips of bEnd.3 cells were stained for MMP9 (red) and DAPI (blue) as a nuclear stain following treatment with increasing doses of rTGFβ1. (C) Quantification of MMP9 immunofluorescence of bEnd.3 coverslips following treatment with rTGFβ1. The data from mRNA and immunofluorescence quantification analyses are reported as mean ± SEM. *=$p<0.05$ compared to basal bEnd.3 cells.

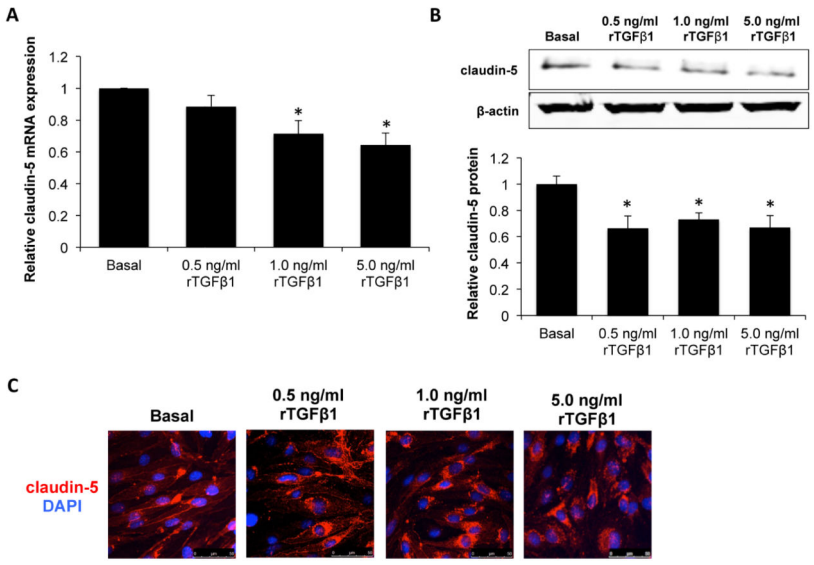

Figure 4. Claudin-5 expression is downregulated in bEnd.3 cells by TGFβ1

(A) Claudin-5 mRNA expression in bEnd.3 treated with indicated doses of rTGFβ1 as assessed by qPCR. (B) Claudin-5 representative immunoblot and quantification in bEnd.3 cells treated with indicated doses of rTGFβ1. β-actin is used as a loading control and quantifications are normalized to basal bEnd.3 cells. (C) Claudin-5 immunofluorescence (red) in bEnd.3 cells treated with rTGFβ1. DAPI (blue) was used to stain nuclei. The data from mRNA and protein analyses are reported as mean ± SEM. *=$p<0.05$ compared to basal bEnd.3 cells.

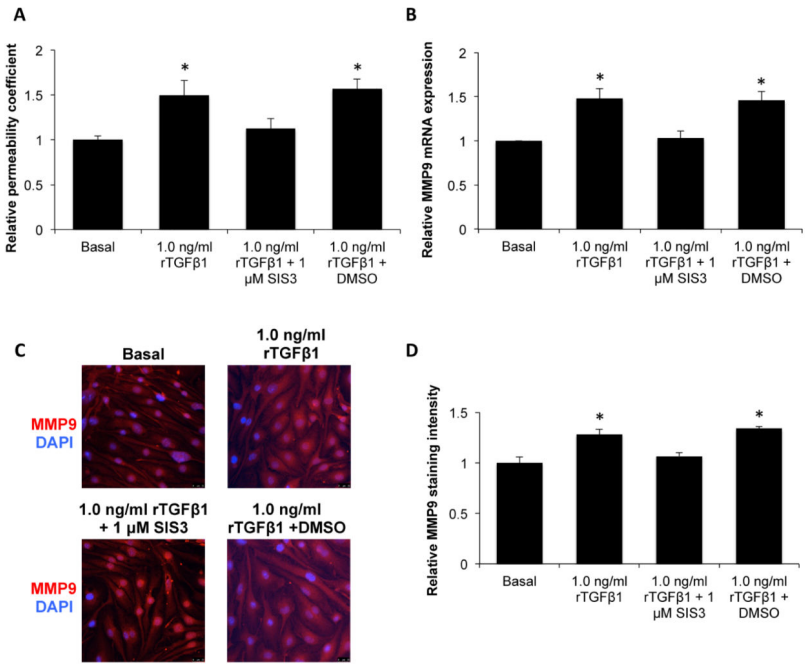

Figure 5. SMAD3 is required for upregulation of MMP9 by TGFβ1

(A) Monolayers of bEnd.3 cells were treated with rTGFβ1, the SMAD3 inhibitor SIS3, or SIS3 vehicle (DMSO) for 24 hours. Permeability was assessed by measuring diffusion of 10-kDa FITC-dextran from the top chamber to the bottom chamber and a subsequent fluorescence measurement (Excitation 494/Emission 520). (B) Relative MMP9 mRNA expression in bEnd.3 cells treated with rTGFβ1, the SMAD3 inhibitor SIS3, or SIS3 vehicle (DMSO) for 24 hours. (C) bEnd.3 cell coverslips were treated with rTGFβ1, the SMAD3 inhibitor SIS3, or SIS3 vehicle (DMSO) for 24 hours. Immunofluorescence against MMP9 (red) and DAPI (blue) were performed. (D) Quantification of MMP9 immunoreactivity on bEnd.3 coverslips following treatment with rTGFβ1 and the SMAD3 inhibitor SIS3. The data from permeability, mRNA and immunofluorescence quantification analyses are reported as mean ± SEM. *=$p<0.05$ compared to basal bEnd.3 cells.

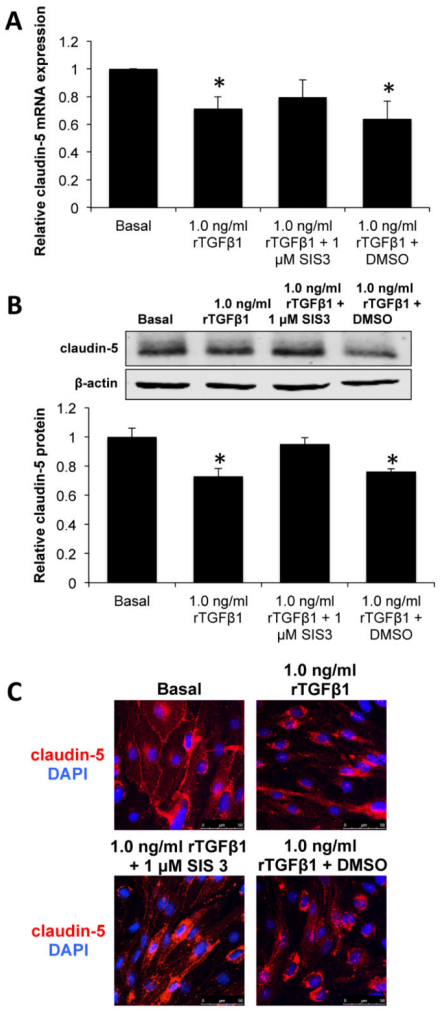

Figure 6. Claudin-5 downregulation via TGFβ1 occurs through a SMAD3-dependent mechanism

(A) Claudin-5 mRNA expression in bEnd.3 cells treated with rTGFβ1, the SMAD3 inhibitor SIS3, or SIS3 vehicle (DMSO) for 24 hours. (B) Claudin-5 protein in bEnd.3 cells treated with rTGFβ1, the SMAD3 inhibitor SIS3, or SIS3 vehicle (DMSO) for 24 hours as assessed by immunoblotting. β-actin is used as a loading control and quantifications are normalized to basal bEnd.3 cells. (C) Claudin-5 (red) immunofluorescence in bEnd.3 cells treated with rTGFβ1, the SMAD3 inhibitor SIS3, or SIS3 vehicle (DMSO) for 24 hours. DAPI (blue) was used as a nuclear stain. The data from mRNA and immunoblot analyses are reported as mean ± SEM. *=$p<0.05$ compared to basal bEnd.3 cells.

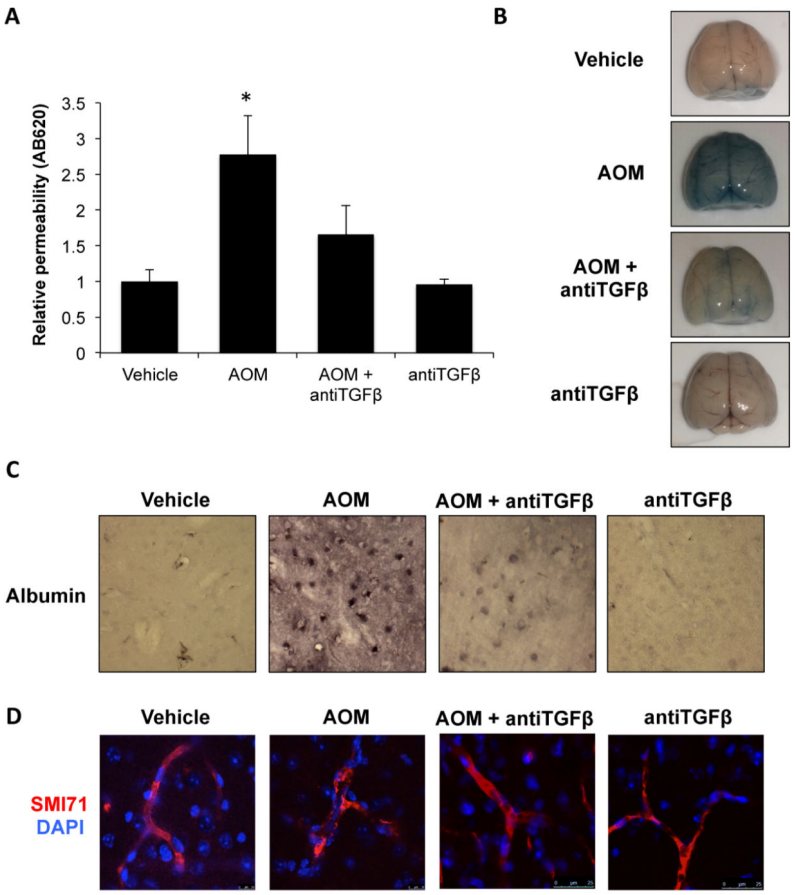

Figure 7. Treatment of AOM mice with neutralizing antibodies against TGFβ reduces BBB dysfunction

(A) Evan's blue dye permeability assay of mice treated with AOM or with neutralizing antibodies against TGFβ for 18 hours (n=4). Permeability was measured by measuring absorbance of Evan's blue dye (620 nM). (B) Representative images of Evan's blue dye extravasation in vehicle, AOM, AOM + antiTGFβ, and antiTGFβ mice. (C) Immunohistochemistry against albumin in the cortex of vehicle, AOM, AOM + antiTGFβ, and antiTGFβ mice. (D) Immunofluorescence staining for the endothelial cell marker SMI71 (red) with DAPI (blue) used as a nuclear stain in the cortex of vehicle, AOM, AOM + antiTGFβ, and antiTGFβ mice. Data in the permeability assay are reported as mean ± SEM. *=$p<0.05$ compared to vehicle-treated mice.

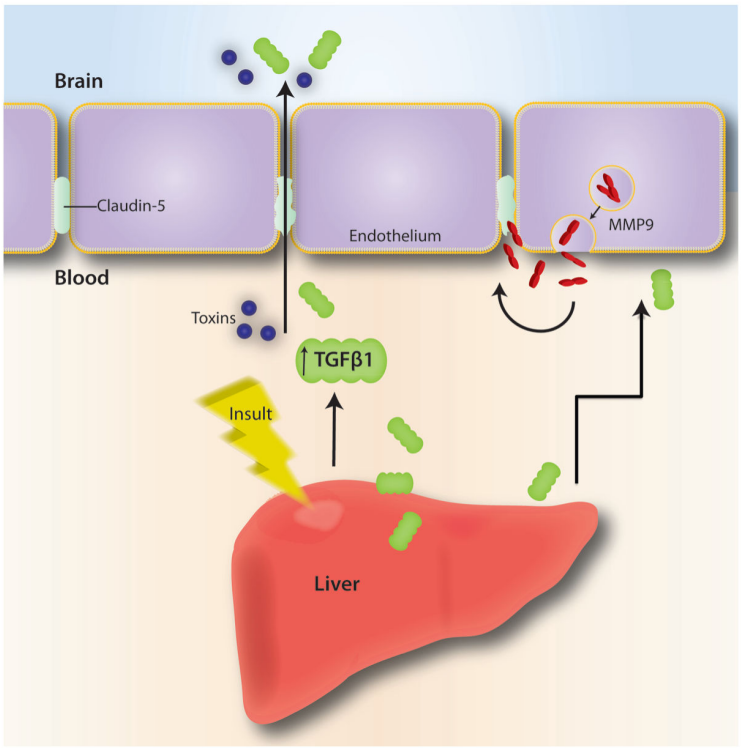

Figure 8. Working model of TGFβ-induced permeability of BBB

Following liver insult, TGFβ1 is released from the liver into the circulation. This generates two subsequent effects. One is the TGFβ1-dependent upregulation of MMP9 in endothelial cells with subsequent release into the circulation and digestion of claudin-5. The other effect is a downregulation of claudin-5 via TGFβ1 and a subsequent disruption of tight junctions. Together these effects allow signaling proteins like TGFβ1 and toxins to pass through the BBB and enter into the brain to exacerbate HE pathology.